Arch. Metall. Mater. **69** (2024), 2, 685-697

DOI: https://doi.org/10.24425/amm.2024.149798

A. SHARMA[1*], S. GUDIKANDULA[1]

THE EFFECTS OF HEAT INPUTS ON LDSS 2101 GTAW AND SMAW WELD MICROSTRUCTURE AND MECHANICAL BEHAVIOR

The welding has been utilized to stabilize the phase fractions in the microstructure of lean duplex stainless steel (LDSS) to build massive mechanical structures. The influence of heat input on the microstructure, mechanical properties, and corrosion behavior of LDSS 2101 during the gas tungsten arc welding (GTAW) and shielded metal arc welding (SMAW) processes is investigated in the present work. Specifically, we compared the outcomes between low heat input (LHI) at 0.85 kJ/mm and high heat input (HHI) at 1.3 kJ/mm for both welding techniques. Throughout the welding process, ER2209 filler wire was utilized. To assess the microstructural changes in the weldments, we employed an optical microscope, a scanning electron microscope, and X-ray diffraction. The results revealed that the volume phase fraction of ferrite was significantly higher in the LHI sample of GTAW compared to HHI GTAW and all SMAW welds. LHI GTAW welds have 18.2% greater Charpy impact toughness than LHI SMAW, whereas HHI GTAW has 35.7% higher than HHI SMAW specimens. The microhardness of the LHI GTAW weldments increased (from 230 ± 3.2 to 252 ± 4.8 HV_{10}), whereas the microhardness of the LHI SMAW weldments increased (from 227 ± 2.8 to 246 ± 5.2 HV_{10}). GTAW exhibited a fine grain structure, showcasing favorable tensile properties and higher hardness compared to SMAW. Conversely, the SMAW welds and their heat-affected regions exhibited coarse grain structures. These findings highlight the superior performance of GTAW in terms of microstructural characteristics, and mechanical properties when working with LDSS 2101 in comparison to SMAW.

Keywords: Gas tungsten arc welding; shielded metal arc welding; Phase fraction; Mechanical properties; LDSS2101

1. Introduction

Duplex stainless steels (DSS) are bi-phase microstructure that contains ferrite and austenite phase fraction with a 50:50 ratio leading to good mechanical properties and corrosion behavior [1]. These steels having good resistance to corrosion are used in environments such as chemical industries, heat exchangers, and paper industries [2-3]. A new DSS, LDSS has low alloying contents of nickel and molybdenum because of the increase in the cost of raw materials. This recently developed LDSS2101 has low Ni (1.5%) content to reduce the cost and stabilize the austenite phase in the microstructure [4-5]. The low nickel alloying element is balanced with the addition of 0.22% nitrogen and 5% manganese to maintain a good microstructure with the balanced phase ratio of ferrite and austenite [6].The element N_2 has been identified as the most potent austenite-generating alloying element. Several authors have pointed out the significance of N_2 in the microstructure evolution [7-10]. Moreover, N_2 serves as a viable and economically efficient substitute for nickel [10]. In addition, Mo content is decreased to limit the deleterious phase precipitation [6]. This steel has increased its industrial application because of the greater yield strength and good localized corrosion resistance than 304 austenitic stainless steel (ASS) [6]. The material strength of LDSS 2101 is comparable to DSS 2205 (UNS S32205) [4]. This alloy has replaced standard austenitic steels in storage tanks and pressure vessels. It provides good corrosion resistance in a sulphate environment as standard Cr-Ni austenitic stainless steel, especially in stress corrosion cracking [11].

In the fabrication industry, joining metals is a critical process with the main objective of ensuring an assembly with the same characteristics as the parent material. It is essential that the mechanical properties and corrosion resistance of the weld joint be maintained at the same level as the base metal. Welding is a well accepted fabrication technique and the fusion welding methods are mostly carried out on DSS [12]. GTAW and SMAW methods are widely used in the welding of structural components and have a good influence on the microstructure

[1] VIT-AP UNIVERSITY, SCHOOL OF MECHANICAL ENGINEERING, AMARAVATI, ANDHRA PRADESH, INDIA-522237

* Corresponding author: sharma.ambuj@vitap.ac.in

of duplex steels in both the weld zone (WZ) and heat-affected zone (HAZ) [13]. GTAW is the conventional fusion welding procedure and is most likely used in DSS manufacture. It has the functional requirements of the weld joint as closest to the base material and has better mechanical properties [14]. SMAW is also a generally used fabrication method that is recognized in all industries because of its simplicity, flexibility, and reliability [15]. The SMAW approach is particularly suitable for positioning welding and enhancing the fabrication quality of joints that have limited accessibility. This is due to the mechanism employed by SMAW, which predominantly utilizes direct current electrode positive (DCEP). The utilization of DCEP in SMAW yields exceptional welding output. The mechanical and corrosion properties of a weldment can undergo significant modifications by the adjustment of input parameters, including voltage, current, welding electrode type, and electrode angle during Welding [16]. SMAW technique has been conducted on welding both similar and dissimilar metals.

Bansod et al investigated the mechanical properties and corrosion behavior on GTAW and SMAW processes for low Ni-ASS. They observed that the tensile strength and microhardness in GTAW are more than SMAW because of high delta ferrite transformation in weld regions of GTAW [13]. The highest Pitting potential and high corrosion resistance are observed in GTAW. Makhdoom et al studied that the tensile and impact toughness of the 2205 in SMAW have decreased than the GTAW. They stated that higher ferrite content in SMAW weldments resulted in low mechanical properties. Also, the corrosion resistance is dependent on the morphological features of different austenite phases and their respective volume phase fractions [17]. Mohandas et al. investigated the comparative analysis of GTAW and SMAW welding techniques on 430 ferritic stainless steel (FSS) and observed that GTAW welding has higher tensile strength and ductility than SMAW [18]. Dhaliwal et al, studied the T91 FSS and 304 ASS using GTAW and SMAW. The impact toughness of the welded joints for GTAW is larger than the SMAW process [19]. The dissimilar weld joint of the GTAW method is observed to be a good weld joint when impact strength is considered. DSS 2205 pipe welds were examined by Li et al. [20], who looked into both GTAW and GTAW+SMAW welds. In a GTAW + SMAW joint, the ferrite content is higher in the WZ and HAZ than in a GTAW joint. A GTAW joint was found to have smaller grain sizes and a more uniform microstructure than a GTAW + SMAW joint.

Higelin et al. investigated and tried to control ferrite content in the HAZ of a DSS grade to enhance weldability. This research described the metallographic approach used to measure ferrite content and the welding outcomes achieved on industrial welds exhibiting very low and steady ferrite concentration in the HAZ [21]. Rokanopoulou et al. [22] have studied and focused on the welding design methods to optimize the phase balance in DSSs during autogenous arc welding under an Ar-N2 environment. They utilized the kinetic model proposed by Du Toit and Pistorius for the evaluation and prediction of the nitrogen's role in the production and stabilization of the austenite phase in welded DSS. To expand the application of LDSS2101 in industries, it is important to achieve suitable mechanical and corrosion properties after the welding process. Gudikandula et al examined the effects of varying heat inputs during GTAW on the microstructural behavior and corrosion of LDX 2101. They observed the reduced hardness when subjected to a high heat input of 1.3 kJ/mm. Under low heat input conditions, the weld metal exhibited a high level of hardness. When comparing the corrosion resistance of weldments, the low-heat welds were shown to be superior compared to high-heat welds [23]. Mortazavi et al. utilized GTAW to manufacture joints between incompatible materials such as austenitic stainless steel (AISI 316L) and high-strength low-alloy steel (API X70) under different heat inputs. These joints were then examined for their microstructure and mechanical properties. The study revealed that as the heat input increased, there was a corresponding rise in both the size of dendrites and interspacing in the weld metal. Furthermore, a reduction was observed in delta ferrite present in the weld metal. Consequently, the tensile strength and hardness were decreased with the increase of the heat input whereas the impact toughness was increased [24].

Verma et al. methodically presented and documented the structure-property connection of DSSs, focusing on the various combinations and emphasizing the impact of welding processes and conditions on microstructure, mechanical properties, and corrosion resistance [8]. Maurya et al. [25] reviewed the challenges of welding DSS to dissimilar materials like nitronic steel (N50) and Inconel 625. Baghel [16] studied a comprehensive assessment of the effect of SMAW process parameters on the quality of stainless steel welds. The ineffective thermal cycles of the fusion welding technique led to the imbalance of phase fractions along the formation of secondary precipitates and intermetallic precipitates which caused the degradation of mechanical properties and reduced the localized corrosion resistance drastically studied by Tan et al. [26], Westin et al. [27], Alvarez et al. [28]. Care must be taken to properly consider the welding process parameters and maintain the required balance of both phases (austenite and ferrite) in weld regions as the microstructural characterization of fusion region and heat-affected regions are strongly dependent on thermal cycle and chemical composition [29-31].

In the present work, two welding techniques termed GTAW and SMAW are performed on LDSS2101 using ER2209 to find the microstructural behavior, and mechanical properties such as ultimate tensile strength (UTS), impact toughness, and microhardness of the weld metal. The aim of the research work is to do a comparative study of the welded microstructures of LDSS2101 for both GTAW and SMAW and evaluate their impact on mechanical properties when varying heat inputs are considered. The experiments are performed taking into account two heat inputs: low heat (LH) with a magnitude of 0.85 kJ/mm and high heat (HH) with a magnitude of 1.3 kJ/mm. The current study does not incorporate intermittent heat input due to the absence of substantial findings from previous research endeavors [32-33]. Both the cooling rate and the change in phase fractions, which affect the microstructural alterations, are also studied.

2. Materials and methodology

2.1. Base Metal and Filler Wire

The LDSS 2101 was used for the present research work. The base material was machined to 200 mm × 100 mm with 8 mm thick using wire-cut Electrical Discharge Machining (EDM) prior to welding. GTAW and SMAW welding processes are performed using a filler wire ER2209 of diameter 3.15 mm to produce the weld joints. The elemental composition of the base material and the filler wire is shown in TABLE 1.

TABLE 1

Elemental composition of -LDSS 2101 and filler material ER 2209

Sample	C	Cr	N	Mn	Cu	Si	Ni	Mo	P
LDSS2101	0.031	21.24	0.24	4.78	0.32	0.68	1.52	0.35	0.03
ER 2209	0.03	21.8	0.13	1.0	0.01	0.9	6.8	3.1	0.026

2.2. Welding Process and Strategy

A single V-groove with 60° with a 2 mm root gap and root face was prepared with machining before welding the samples. Considerable attention was devoted to the meticulous cleansing of the joint edges by the implementation of a solitary V-groove. The welds were produced via a mechanized welding stand including a semi-automatic welding machine and a welding trolley equipped with a torch capable of accurately adjusting the travel speed. The experiment utilized a continuous flow rate of 11 L/min of pure argon gas, in accordance with the standard EN ISO 14175-I1-Ar, for the purpose of shielding. The specimens were not subjected to any pre or post-heat treatment. Throughout the welding process, a thorough visual examination was conducted on the joints to verify that all weld beads displayed desirable geometrical uniformity and were free of any observable flaws. The welding process employed for joining the LDSS 2101 plate, which had a thickness of 8 mm, involved the use of multipass welding with a total of 5 passes. The initial pass was performed under ambient temperature conditions, but the succeeding runs were executed at temperatures exceeding 150°C. The weld joints were specifically produced with two distinct welding currents, namely 74 A and 86 A, with the intention of achieving low heat input and high heat input, respectively. The suitable welding parameters for GTAW and SMAW methods are shown in TABLE 2. At -74 A, the computed heat input is 0.85 kJ/mm, which is considered LHI, and for 86 A the computed heat input is 1.3 kJ/mm, which is considered HHI for both GTAW and SMAW processes. For DSS, the range of arc energy that can be used in industry is between 0.5 and 2.5 kJ/mm (estimated with a thermal efficiency of 1.0) [34]. The schematic of the weldment is shown in Fig. 1. These welds are labeled in TABLE 3 so that they can be easily identified.

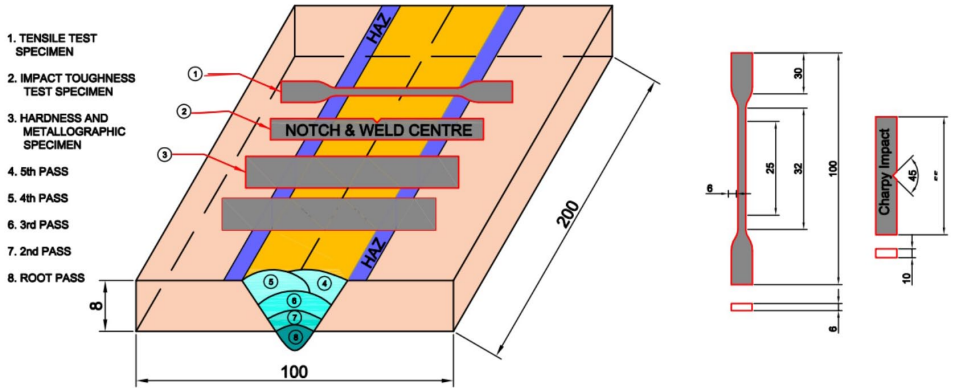

Fig. 1. Schematic of weldments and samples extraction

TABLE 2

Welding process parameters for low and high heat inputs

Sample	Current (A)	Voltage (V)	Heat input (kJ/mm)	Electrode diameter (mm)	Root gap (mm)	Plate distance (mm)	Weld time (Sec)
LHI	74	21	0.85	3.15	2	100	55
HHI	86	25.2	1.3	3.15	2	100	60

TABLE 3

Designation of the test specimens

Specimen designation	Description	Heat inputs	Welding Current
LHIG	Low heat input GTAW weld	0.85 kJ/mm	74 A
HHIG	High heat input SMAW weld	1.3 kJ/mm	86 A
LHIS	Low heat input GTAW weld	0.85 kJ/mm	74 A
HHIS	High heat input SMAW weld	1.3 kJ/mm	86 A

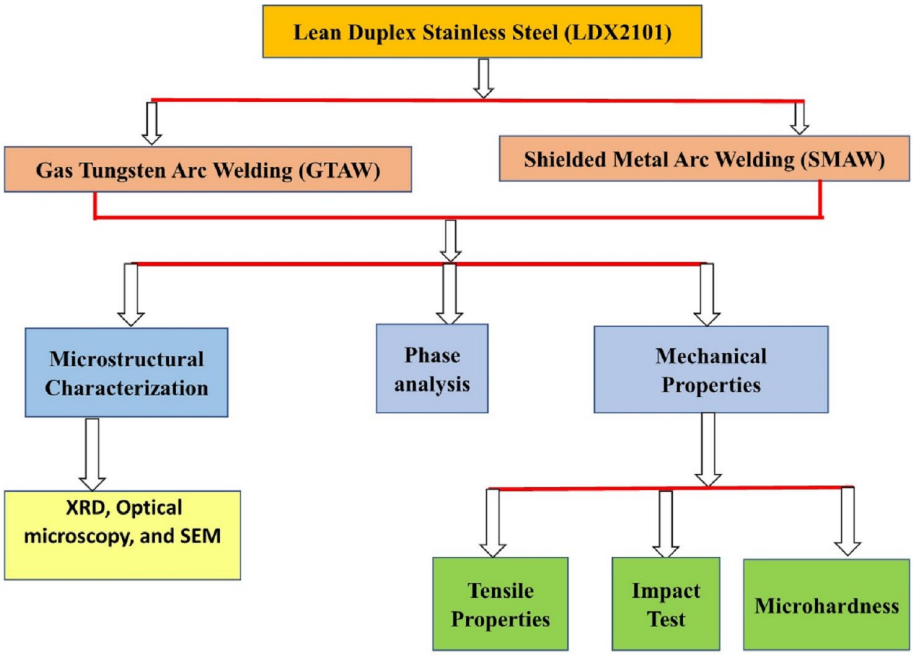

Fig. 2. Characterization approach of weldments used in the present study

GTAW and SMAW samples with a low heat input are labeled LHIG and LHIS, respectively. The notations HHIG and HHIS denote welds produced with a high heat input for both GTAW and SMAW. Fig. 2 shows the characterization approach of weldments used in the present study.

2.3. Characterization Approach of Weldments

The samples were polished using emery sheets (180, 200, 400, 600, 800, 1000, 1100, and 1200 grit) and diamond polish according to ASTM E3-95 for microstructural characterization. Kallings reagent (CuCl2-5 gms, HCL-100 ml, C2H2OH-100 ml) was used to etch these polished samples for 10-20 sec before they were examined for microstructural alterations. The different weld regions of all samples were analyzed using OLYMUS makes optical metallurgical microscope and TESCAN makes scanning electron microscope (SEM) attached energy dispersive spectrum software for localized elemental composition. X-ray diffraction (XRD) is done for the identification of different phases welded samples using Bruker D2 Phase 2nd generation with Cu (Ka) radiation operated at 40 kV and 40 mA. The resulting peaks are analyzed using Xpert High Score software using the PDF4 database. Samples for measuring the mechanical properties are prepared from the welded joints using EDM to analyze the effect of microstructural evolution on the mechanical behavior of the weldments. Tensile, impact, and microhardness tests were carried out according to ASTM standards. A tensile strength test was performed on SHIMADZU make Model-343-07979-12, capacity 250 kN at ambient temperature with a strain rate of 2 mm/min. A charpy impact toughness test was performed at room temperature to determine the impact toughness of welded samples. Fractography analysis was carried out on tensile and impact samples to examine the type of failure with the characteristics of fractured surfaces. Microhardness analysis was carried out on the Vickers Hardness Tester (METCO VH-1MDX) to evaluate the material resistance to indentation. A 10kg load is released and applied slowly through the indenter for 10-15 sec on the specimen surface to measure microhardness. The corrosion performance of the weldments was studied using the potentiodynamic polarization method by employing a conventional 3-electrode cell. Prior to the electrochemical test, the samples were immersed in 3.5% NaCl solution at 350°C for 30 minutes and the scanning rate was kept at 10 mV/s to conduct the polarization test. The surface area of samples exposed to the solution was 0.1257 cm^2.

3. Results and discussions

3.1. Metallography behavior of GTAW and SMAW

The optical and SEM microstructures of the BM are shown in Fig. 3. It is noticed that the BM is a two-phase microstructure consisting of ferrite and austenite phases. The austenite phase is seen as a light-etched banded region which is discontinuous and the ferrite phase is observed to be a continuous dark matrix and the ratio of phase fraction is close to 1:1 [26]. The microstructures of the welded regions are difficult to analyze as rapid heating and cooling take place in fusion welding processes such as GTAW and SMAW. In the present study, the solidification mode for both GTAW and SMAW was observed to be ferrite-austenite mode. Fig. 4 represents the optical micrographs of weldments obtained from GTAW and SMAW processes. Fig. 4(a-b) depicts the macrostructure of weldments produced at low heat input GTAW and SMAW respectively. Fig. 5(a-b) – displays the similarities between the microstructures of welds, including the presence of

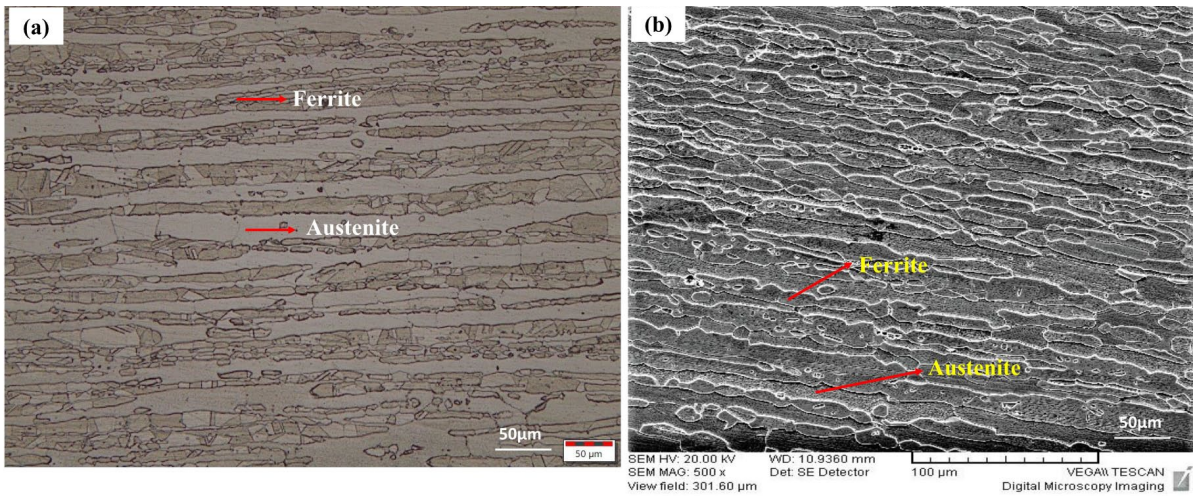

Fig. 3. Base material LDSS 2101 micrograph (a) optical image (b) SEM image

grain boundary austenite (GBA), inter-granular austenite (IGA), and Widmanstatten austenite (WA). Grain boundary austenite (GBA) is nucleated at ferrite grain boundaries during weld cooling, where it grows into a ferrite grain with certain angles after being followed by Widmanstatten secondary austenite. At last, the IGA crystallized within the ferrite grains. The final microstructure is determined by the extent of under-cooling [23,32,25-27]. From both GTAW and SMAW weldments, it was observed that the α-ferrite phases remain stable and austenite (γ) phases are dissolved in it during high thermal cycles. The welded microstructures exhibited a wide variety of austenite morphologies. Both procedures resulted in microstructures free of intermetallic and secondary phase precipitates, and the welded samples exhibited good austenite phase change as WA, GBA, and IGA. Fig. 5(c-d) – shows the optical image of the interface of HAZ/BM and WZ for both processes. The welded microstructural behavior is a result of the predicted heat input and cooling rate. Results from microstructural analysis of both welding processes showed that at lower heat input (0.85 KJ/mm), weldments cooled more quickly, resulting in higher ferrite levels and finer grains, while at higher heat input (1.3 kJ/mm), weldments cooled more slowly, leading to higher austenite contents and coarser grains [17].

Fig. 6 displays the typical percentage of ferrite and austenite fractions in LHI and HHI weldments produced by GTAW and SMAW. The determination of volume fractions of identifiable phases within the WZ was conducted for both heat sources. The approach utilized the commercial software known as Biovis. The determination of the volume phase fraction was conducted in accordance with the guidelines outlined in ASTM E562. This involved calculating the phase area and subsequently deriving the volume phase fraction. At LHI and HHI, ferrite levels were 55.87% and 47.31% for GTAW weldments, and 52.1% and 46.9% for SMAW weldments. δ-ferrite formation in the weld regions is purely dependent on the cooling rate of welding. Increased heat input is associated with a decrease in the ferrite phase fraction in the WZ [35]. Therefore, LHIG samples have high ferrite content because of a faster cooling rate and indirectly facilitate low austenite formation. SEM images of GTAW and SMAW welds are displayed in Fig. 7. Fig. 7(a-b) displays the microstructural distinction between LHIG and HHIG. Micrographs of the SMAW samples' microstructure are shown in Fig. 7(c-d). It was observed that the microstructure of the welded sample exhibited a variation in the grain morphology when compared to the BM. Also, it was noticed that the new coarse grains are formed due to the insufficient GBA phase in the HHI

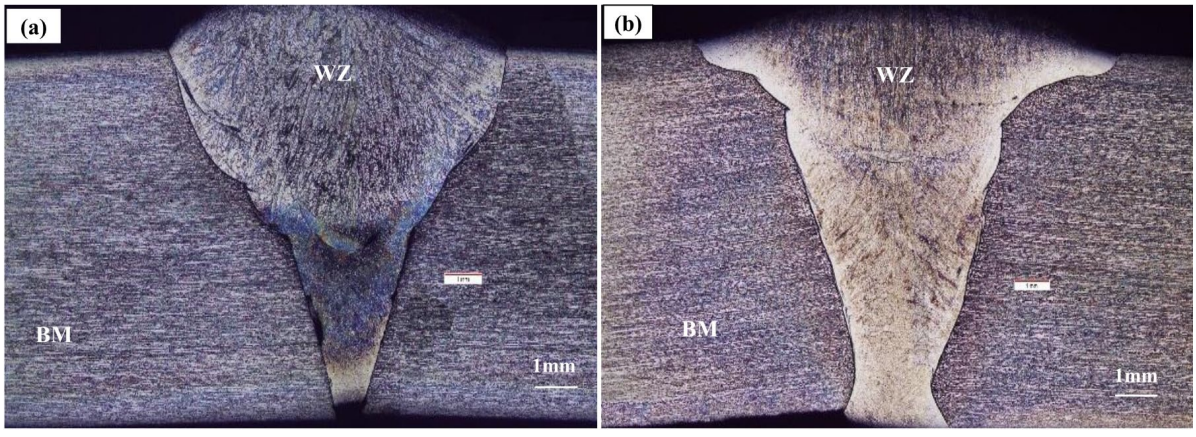

Fig. 4. Optical micrographs of weldments (a) GTAW weld (b) SMAW weld

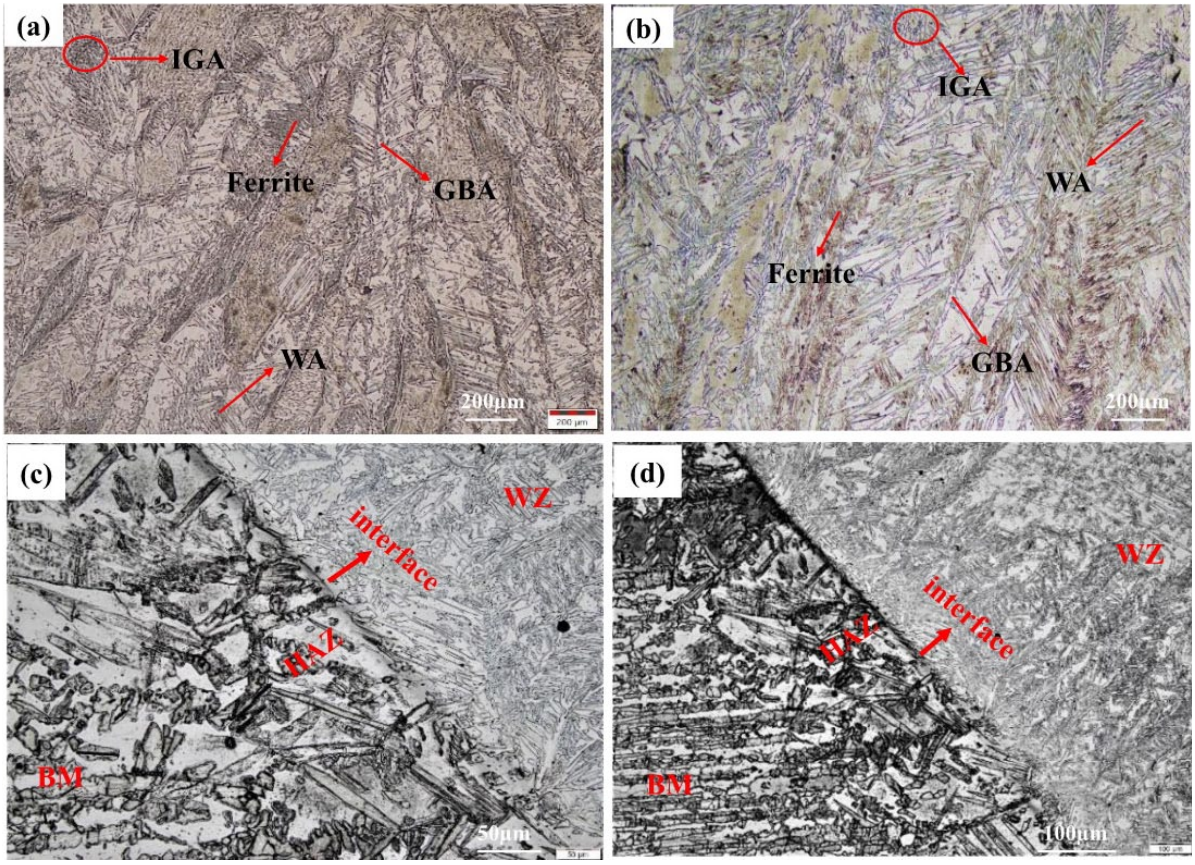

Fig. 5. Optical micrographs of weldments (a) GTAW WZ (b) SMAW WZ (c) interface of GTAW (d) interface of SMAW

weldments. These changes in the morphological characteristics of the weldments compared to BM are due to the change in the elemental composition of the welded joint. The welding cooling rate is also an important aspect that influences the morphology of welded joints. The grain growth during the welding process is dependent on the heat inputs.

EDS measurements were carried out on both GTAW and SMAW weldments to find the elemental composition at HAZ and WZ. TABLE 4 displays the most common alloying sub-

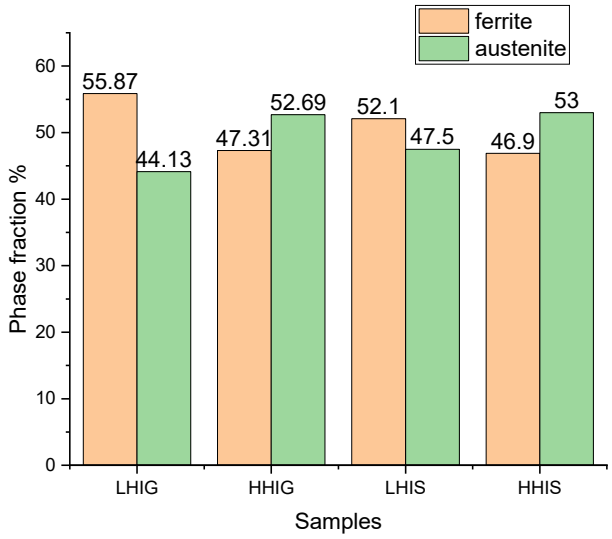

Fig. 6. Phase analysis of welded samples

TABLE 4

EDS analysis of GTAW and SMAW

Sample	Zone	Cr	Ni	Mn
BM		21.35	2.26	**6.03**
LHIG	WM	23.93	7.46	**2.20**
	HAZ	22.04	1.67	**4.97**
HHIG	WM	23.71	8.29	**2.26**
	HAZ	22.57	2.27	**4.84**
LHIS	WM	22.5	8.01	**2.78**
	HAZ	21.96	1.90	**7.08**
HHIS	**WM**	**21.77**	**6.90**	**2.30**
	HAZ	**22**	**1.93**	**6.09**

stances. A shift in the chromium concentration from WZ to HAZ was observed. The WZ of the LHIG sample had a higher Cr level than the others. The Cr concentration of HHIG, LHIS, and HHIS elements decreased respectively in the WZ. In all samples, Ni element content was found to be greater in the weld areas than in the HAZ.

Fig. 8 shows the comparison of X-ray diffraction peaks of BM with all welded samples. It is evident that for all welding processes, the occurrence of sharp peaks is attributable to the γ-austenite and δ-ferrite phases. The LHIG weld exhibited well-balanced phases with high {111} plane orientation which correlates nicely with the findings of reference [32]. It can be also seen that δ-ferrite with {2 0 0} plane orientation is prominent in the LHIG weld as compared to other weldments.

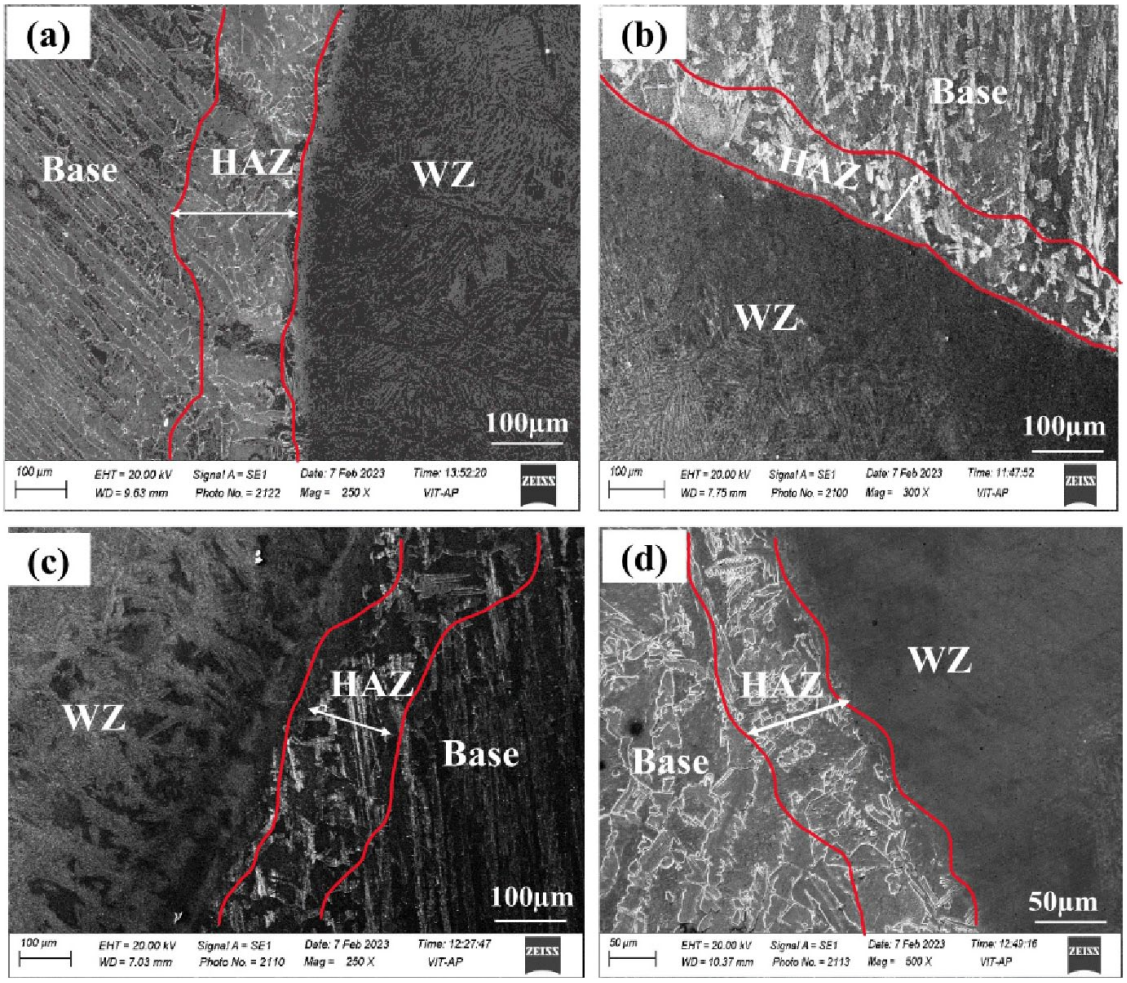

Fig. 7. SEM images of GTAW and SMAW weldments at the interface of HAZ/BM and WZ:(a) LHIG (b) HHIG (c) LHIS (d) HHIS

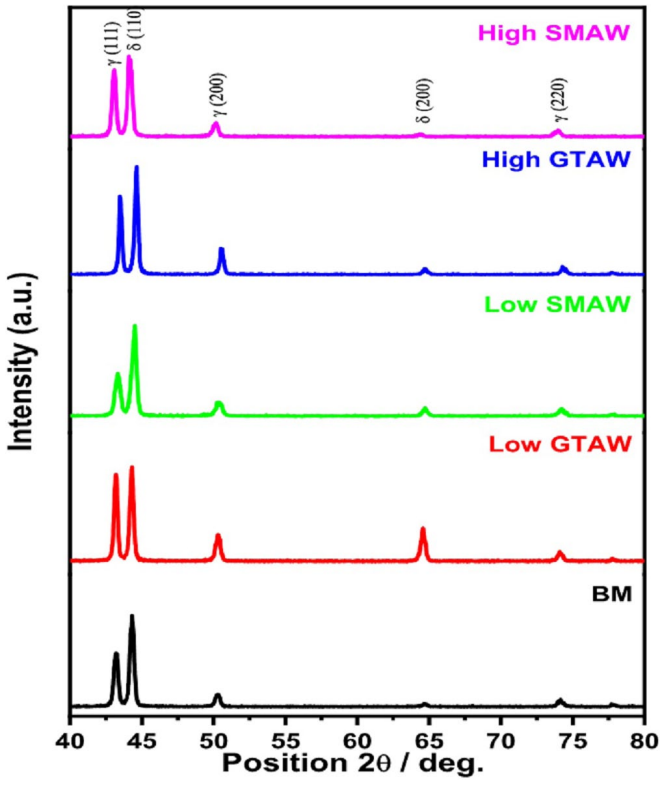

Fig. 8. Comparison of XRD peaks of base and welded samples

Nonetheless, the peak intensity of the ferrite phase reduced in comparison to the austenite phase in the high-heat input weldments, demonstrating the phase transformation from the ferrite to austenite. This indicates the conversion of the ferrite phase to the austenite phase. This may be ascribed to the elevated nickel concentration present in the filler metal ER 2209, as well as the prolonged duration required for the transformation of δ-ferrite into γ-austenite, which is directly influenced by the heat input. However, as can be seen in Fig. 8 of the XRD spectra, the weldments do not contain any secondary precipitates or detrimental phases, such as the σ phase or carbides, that could otherwise be expected to be present. The results of this investigation confirm that LDSS 2101, which contains low concentrations of chromium and molybdenum, displays less susceptibility to phase development and exhibits significant stability in preventing the formation of secondary phases.

3.2. Mechanical behavior

3.2.1. Tensile Strength

Welding causes a change in microstructure and a phase transition, both of which have an effect on mechanical charac-

teristics. TABLE 5 displays the average of the tensile testing results. The ultimate tensile strength (UTS) of the base material was 680 MPa, whereas the weldments LHIG, HHIG, LHIS and HHIS were 705 MPa, 691 MPa, 681 MPa and 626 MPa respectively. The UTS of GTAW welds is 1.6-3.7% higher than the BM. The LHIS welds have a significantly lower UTS when compared to the GTAW samples, but they are comparable to the BM. However, as compared to the other samples, HHIS welds display the lowest levels of UTS. The tensile strength is recorded higher when heat is lower than others due to the high cooling rate with refined grains [36]. The increase of UTS in LHIG and LHIS samples is because of the high ferrite fraction in the weld region which gave good strength to the weld [13]. The yield strength of LHIG, HHIG, LHIS and HHIS samples were noted as 528 MPa, 504 MPa, 538 MPa and 501 MPa respectively. The filler ER2209, which is based on nickel, helps to strengthen the strength of the weldment. As a result, the yield strength of low-heat weldments is greater than the BM. The GTAW and SMAW weldments were found to have a lower % elongation than the BM, between 5% and 10% for GTAW and between 10% and 15% for SMAW. The UTS of the samples is illustrated in Fig. 9(a). Fig. 9(b) illustrates the relationship between the yield strength and the elongation of the material.

Fractography analyses were carried out to understand the failure behavior of the base and weldments and these are shown in Fig. 10. The necking phenomenon at the fracture location indicated that the tensile specimens had deformed plastically before fracture. Fig. 10(a) shows a fractography of the BM. Tinny dimples are visible throughout the surface indicating the ductile mode of fracture. During the tensile test, all the weldments are fractured from HAZ to the weld region with the mix mode (ductile and brittle) of fracture. Fig. 10(b) presents the fractography of the GTAW process, whereas Fig. 10(c) illustrates the fractography associated with the SMAW technique. Dimples of different sizes and shapes as well as small tearing ridges are observed in the fractured surface of both GTAW and SMAW weldments. The fractured surfaces are ductile morphology and some grains with brittle behavior. The cleavage facets and micro-voids are also present in all the weldments that confirm to the mix mode of failure. LHI weldments display more uniform small and shallow dimples as compared to HHI welds which indicates the good strength and ductility of the weldment. Coarse and elongated dimples are populated over the entire fracture surface with micro-voids in the HHI weldments because of increased heat input. The material strength is increased due to the bi-phase microstructure which led to the formation of fine grains.

3.2.2. Impact Toughness

The impact test was performed on the weld region centerline for both GTAW and SMAW processes. In order to ascertain the average impact toughness of the weldments, three specimens were analyzed for each welding energy level. The impact toughness of the samples is tabulated in TABLE 6. The average toughness of LHIG, HHIG, LHIS and HHIS were noted as 125 J, 76 J, 105.7 J and 56 J respectively. Fig. 11 shows the impact toughness of the weldments. It is observed that, when

TABLE 5

Tensile – results of GTAW and SMAW

Specimen	UTS (MPa)	YS (MPa)	% Elongation	Fracture location	Fracture Mode
Base	680	495	28.07%	Centre of gauge	Ductile
LHIG	705	528	25.3	HAZ Weld	Mixed mode of (ductile + brittle)
HHIG	691	504	26.8	HAZ Weld	Mixed mode of (ductile + brittle)
LHIS	681	538	22.86%	HAZ Weld	Mixed mode of (ductile + brittle)
HHIS	626	501	20.12%	HAZ Weld	Mixed mode of (ductile + brittle)

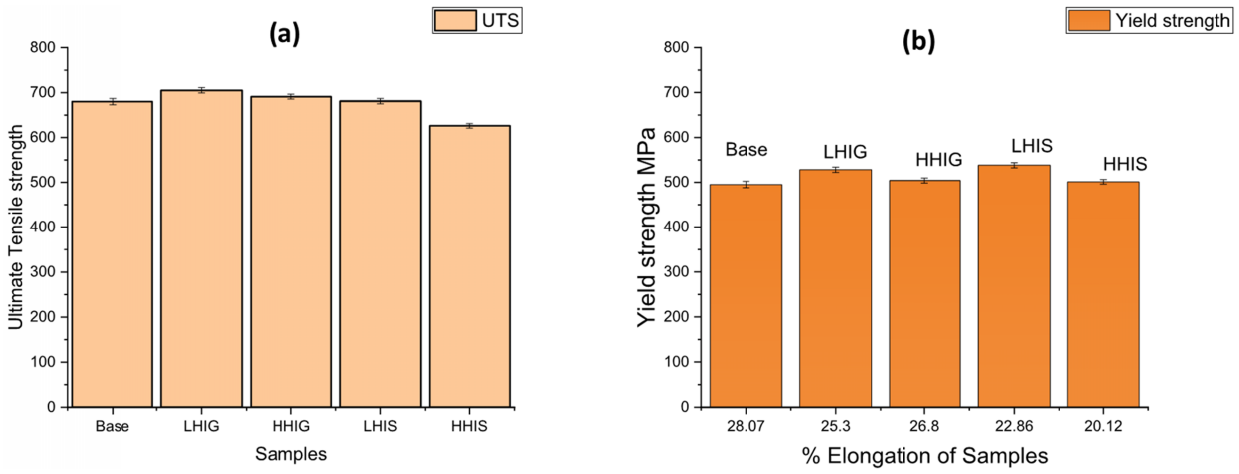

Fig. 9. (a) UTS of the BM and weldments (b) yield strength of the BM and weldments vs elongation

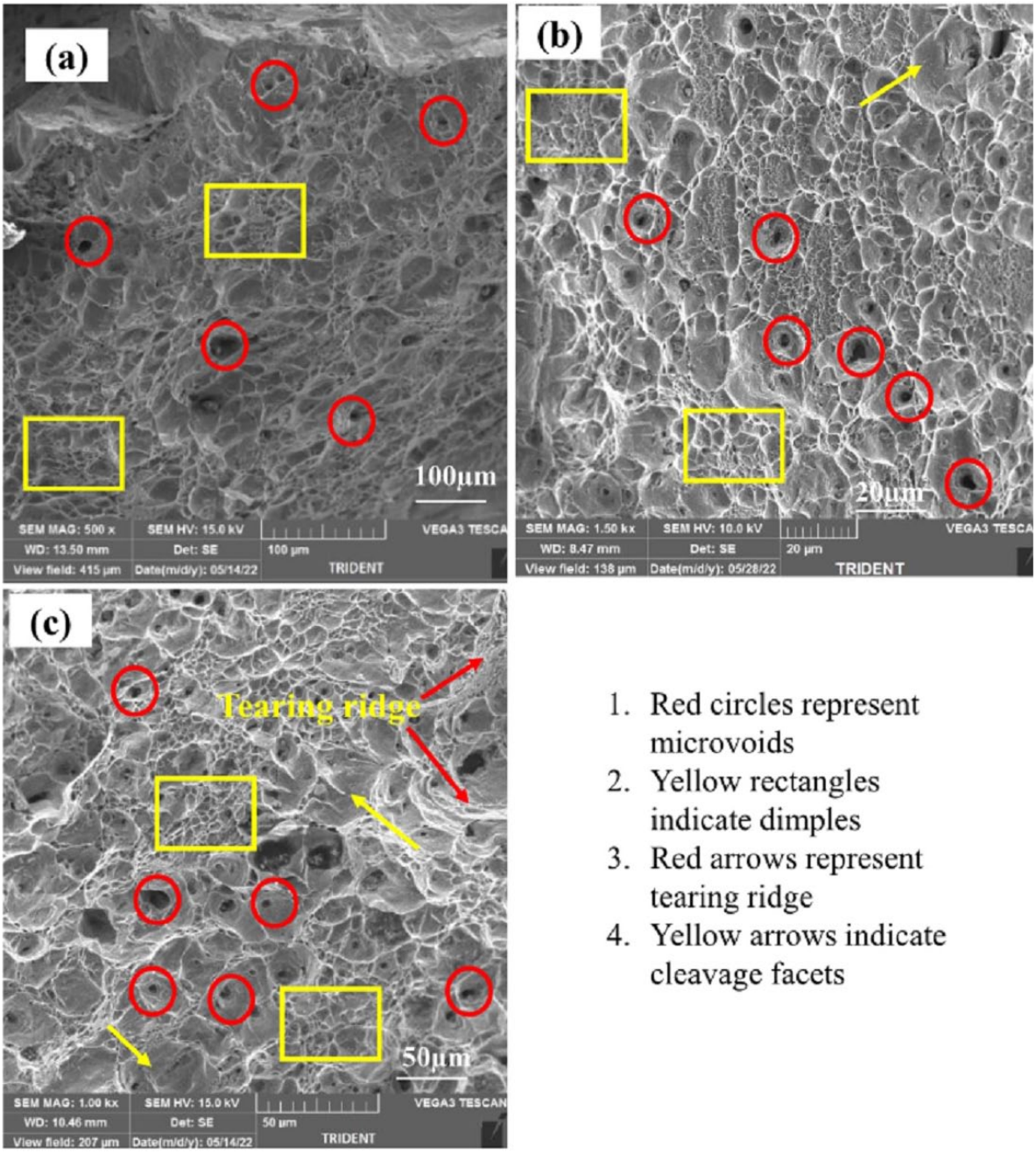

Fig. 10. Tensile fractography of samples (a) BM (b) LHIG (c) LHIS

TABLE 6

Impact test results of GTAW and SMAW samples

Samples	Avg. impact energy (J)	Max impact energy (J)	Min impact energy (J)	Fracture mode	Standard error	Notch location
LHIG	125	137.3	102.7	Mix mode of fracture	11.16	Weld notch
HHIG	76	81.6	66.5	Mix mode of fracture	4.76	Weld notch
LHIS	105.7	128.6	92.4	Mix mode of fracture	11.4	Weld notch
HHIS	55.68	63.4	43.7	Mix mode of fracture	6.14	Weld notch

welding is carried out at different heat inputs, not only strength has improved but also the toughness has improved in GTAW than SMAW. The high impact toughness in the LHI samples is due to the cooling rate and the high arc energy [37]. The refined grain structures in LHI weldments of both processes are also the reason for higher toughness compared to HHI samples. The grain coarsening resulted in the loss of toughness in HHI welds. SMAW samples have less impact toughness than GTAW samples. The observed toughness differences might also be because of the reduced ferrite-to-austenite ratio [38].

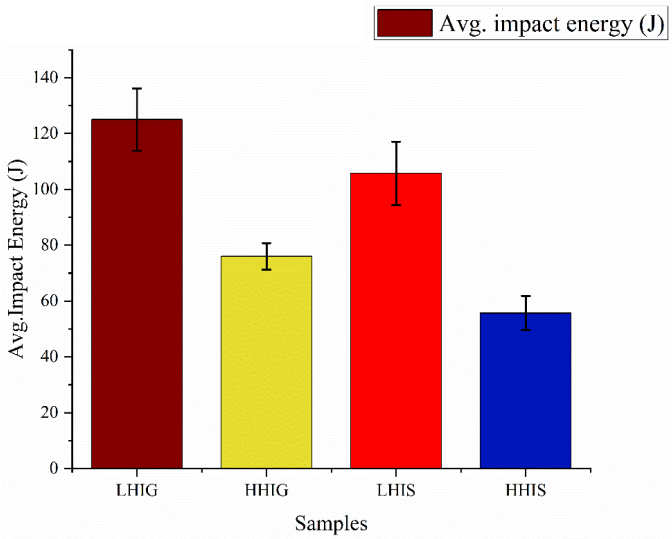

Fig. 11. Impact toughness of all welded samples

The fractography analysis of impact fractured samples is shown in Fig. 12. It is observed that the specimens are ductile fractured after the Charpy impact test. The presence of small dimples on the fracture surface of BM after the impact toughness test is consistent and can be observed in Fig. 12(a). The fracture surface of LHIG weld is characterized by ductile fracture, with fine dimples, small tearing ridges, micro-voids, and less brittle grains shown in Fig. 12(b). In the case of SMAW welds, the fractography revealed a mixed mode of fracture. The fracture surface exhibited ductile fine shallow dimples, small cleavage facets, tearing ridges, and micro-voids, as observed in Fig. 12(c).

3.2.3. Micro Hardness

The microhardness of all weldments is compared and seen in Fig. 13. The hardness values in weld regions of LHIG, HHIG,

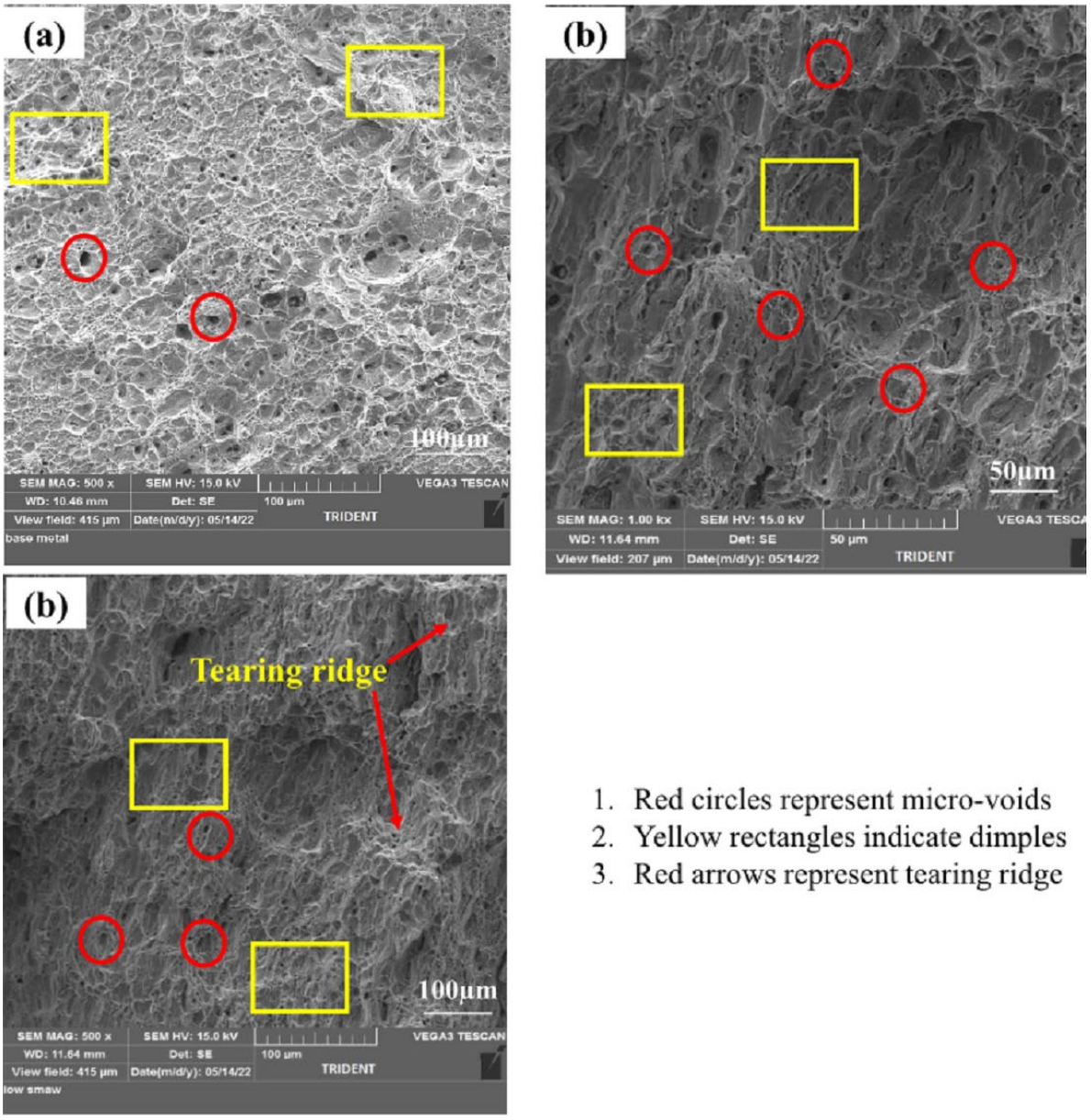

1. Red circles represent micro-voids
2. Yellow rectangles indicate dimples
3. Red arrows represent tearing ridge

Fig. 12. Impact fractography of low GTAW and low SMAW samples

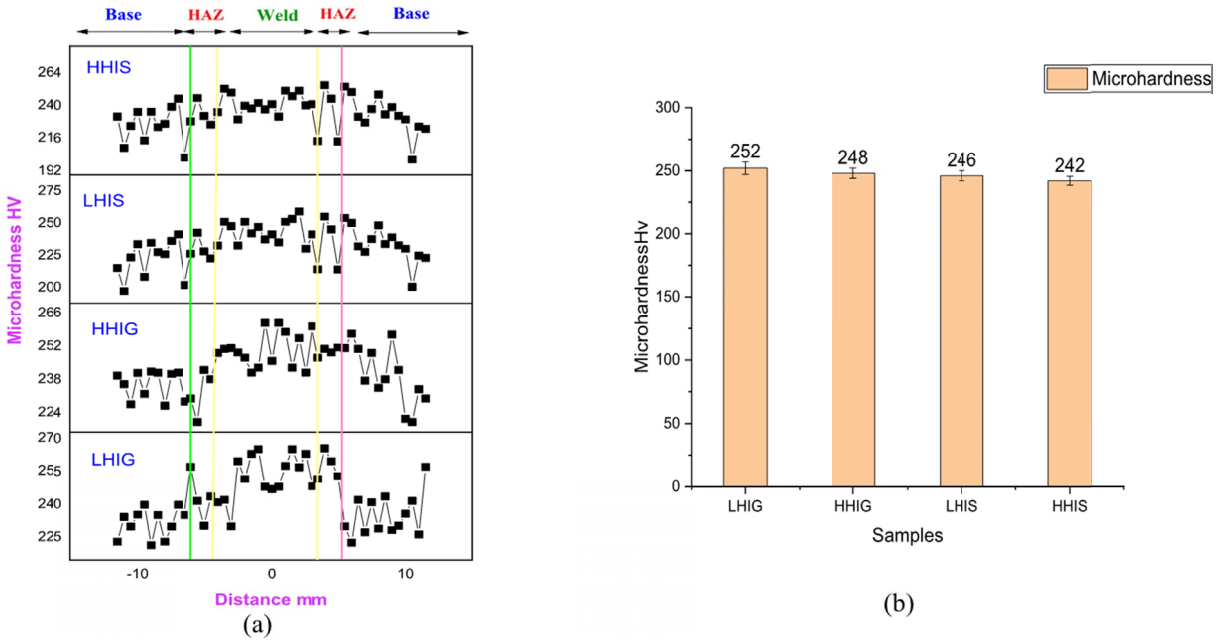

Fig. 13. Comparison of microhardness values of weldments (a) BM, HAZ, WZ (b) average microhardness in WZ

LHIS and HHIS samples were 252 HV, 248 HV, 246 HV and 242 HV respectively. The microhardness of BM, HAZ, and WZ are shown in TABLE 7. It is observed that weld region hardness decreased with increased heat input for both weldments. This decrease in hardness from LHI to HHI in the weld region is due to the cooling rate difference and the phase fraction. As heat input increases, the cooling rate decreases and results in an increase of the γ-austenite formation, leading to a reduction in hardness performance [39]. This led to the decrement of the ferrite contents in the weld region. It is observed that for LHI welding, the ferrite-austenite transformation is less in comparison to high heat welding because of the fast-cooling rate in LHI welding [40]. It can be noticed that the weld region has higher hardness value than HAZ and BM for both weldments because of the fine grain size in the weld region. The microhardness values of GTAW are reported to be higher than SMAW welding process which is because of the higher δ-ferrite fraction in the weld regions of GTAW welding (Fig. 13(b)) [41]. The micro hardness of the weldments is influenced by the change of alloying elemental composition during welding.

TABLE 7

Microhardness in different regions

Sample	BM	HAZ	WZ
LHIG	230	237	252
HHIG	240	239	248
LHIS	227	231.2	246
HHIS	232	235	242

4. Conclusions

In the present study, we conducted an investigation into the effects of varying heat inputs in GTAW and SMAW on the microstructural characteristics, mechanical properties, and corrosion behavior of -LDSS 2101. A comparative analysis was performed using LHI of 0.85 kJ/mm and HHI of 1.3 kJ/mm for both welding processes. Throughout the welding process, ER2209 filler wire was consistently employed. The conclusions drawn for both processes are as follows.

i. The metallurgical testing of weld samples showed the formation of GBA, IGA and WA for both GTAW and SMAW weldments. The phase analysis of weldments showed that when heat input is 0.85 kJ/mm, the ferrite fraction is high. The LHI GTAW weld displayed higher ferrite levels due to the less time for austenite reformation.

ii. In the WZ of the LHI GTAW weld, greater chromium concentrations were discovered using EDS analysis, and no secondary precipitates or intermetallic phases were found using XRD analysis.

iii. The tensile strength and ductility of the weld metal were affected by the ferrite content and grain sizes. LHI GTAW Weld metal has a maximum UTS of 705 MPa, which is greater than the base metal.

iv. The impact toughness is higher in the LHI GTAW samples as compared to other weldments due to the more δ-ferrite in WZ. This is due to the cooling rate during welding where the finer grains are attained when heat input was 0.85KJ/mm which is lower and had a fast cooling rate. Fractography analysis revealed the mixed mode of fracture for all weldments.

v. The findings of the microhardness test showed that as the heat input was increased, the hardness of the weldment dropped. The WZ of both welding procedures reported high hardness compared to BM and HAZ due to the elemental composition of the material during welding and volumetric phase fraction.

vi. These findings contribute to a better understanding of the influence of heat inputs in GTAW and SMAW on the

microstructural, mechanical, and corrosion characteristics of LDSS 2101. This research has important implications for optimizing welding processes and selecting appropriate welding parameters for lean duplex stainless steel applications.

Lean duplex 2101 can be welded using GTAW and SMAW process for ER2209 as it has enhanced the morphology. However, welding with the GATW process is recommended due to its better properties as compared with SMAW.

5. Future directions and limitations

Both GTAW and SMAW involve localized heating, which can lead to distortion and residual stresses in the weldments, affecting their dimensional accuracy. Careful control of heat input and the use of proper welding techniques are essential to mitigate these issues. LDSS 2101 is susceptible to the formation of undesirable intermetallic phases during welding, which can degrade the material's mechanical and corrosion properties. Welding parameters, filler material selection, and post-weld heat treatments must be carefully selected to minimize intermetallic phase formation. Ensuring the quality of welds in LDSS can be challenging due to their complex microstructures as well as due to the potential for defects such as porosity, lack of fusion, and cracks. Non-destructive testing methods may need to be developed or refined to accurately assess weld integrity.

Future research might focus on optimizing welding parameters such as voltage, current, and shielding gas composition to enhance the quality and efficiency of GTAW and SMAW on LDSS. These optimizations could lead to improved weld bead appearance, reduced distortion, and enhanced mechanical properties. The development of specialized filler materials for DSS could play a significant role in achieving improved weld properties. These fillers might be engineered to match the chemical composition of LDSS 2101 and provide superior corrosion resistance and mechanical strength. Hybrid techniques, such as laser-assisted welding or electron beam welding in combination with GTAW or SMAW, might be explored to achieve even higher-quality welds with reduced heat affected zones.

REFERENCES

[1] P. Bassani, M. Breda, K. Brunelli, I. Mészáros, F. Passaretti, M. Zanellato, I. Calliari, Microscopy and Microanalysis **19**, 988-995 (2013).
DOI: https://doi.org/10.1017/S1431927613001426

[2] H. Sieurin, R. Sandstrom, Materials Science and Engineering **418**, 250-256 (2006).
DOI: https://doi.org/10.1016/j.msea.2005.11.025

[3] B. Kurt, Journal of Materials Processing Technology **190**, 138-141 (2007). DOI: https://doi.org/10.1016/j.jmatprotec.2007.03.063

[4] J. Olsson, M. Snis, Desalination, **205**, 104-113 (2007).
DOI: https://doi.org/10.1016/j.desal.2006.02.051

[5] T. Oshima, Y. Habara, K. Kuroda, ISIJ International **47** (3), 359-364 (2007).
DOI: https://doi.org/10.2355/isijinternational.47.359

[6] M. Liljas, P. Johansson, H. Liu, C.O.A. Olsson, Steel Research International **79** (6), 466-473 (2008).
DOI: https://doi.org/10.1002/srin.200806154

[7] P. Boillot, J. Peultier, Procedia Engineering **83**, 309-321 (2014).
DOI: https://doi.org/10.1016/j.proeng.2014.09.015

[8] J. Verma, R.V. Taiwade, J. Manuf. Process. **25**, 134-152 (2017).
DOI: https://doi.org/10.1016/j.jmapro.2016.11.003

[9] H.Y. Liou, W.T. Tsai, Y.T. Pan, R.I. Hsieh, Journal of Materials Engineering and Performance **10**, 231-241 (2001).
DOI: https://doi.org/10.1361/105994901770345268

[10] V.A. Hosseini, S. Wessman, K. Hurtig, L. Karlsson, Materials & Design **98**, 88-97 (2016).
DOI: https://doi.org/10.1016/j.matdes.2016.03.011

[11] H. Sieurin, R. Sandström, E.M. Westin, Metallurgical and Materials Transactions. A **37A**, 10, 2975-2981 (2006).
DOI: https://doi.org/10.1007/s11661-006-0179-7

[12] D. Nelson, W. Baeslack, J. Lippold, Materials Characterization **39**, 467-477 (1997).

[13] A.V. Bansod, P. Awani kumar, Metallography Microstructure and Analysis, (2017).
DOI: https://doi.org/10.1007/s13632-017-0368-3

[14] K. Mehta, Advanced Joining and Welding Techniques, An Overview. Materials Forming, Machining and Tribology, (2017).
DOI: https://doi.org/10.1007/978-3-319-56099-1_5

[15] J.C. Lippold, D.J. Kotecki, Wiley Inter science, (2005).

[16] P.K. Baghel, Heliyon **8**, e12161 (2022).
DOI: https://doi.org/10.1016/j.heliyon.2022.e12161

[17] M.A. Makhdoom, A. Ahmad, M. Kamran, K. Abid, W. Haider, Surfaces and Interfaces,
(2017). DOI: https://doi.org/10.1016/j.surfin.2017.09.007

[18] T. Mohandas, G.M. Reddy, M. Naveed, J. Mater. Process. Technol. **94**, 133-140 (1999).
DOI: https://doi.org/10.1016/S0924-0136(99)00092-8

[19] N.P.S. Dhaliwal, R. Mittal, S. Gill, P. Khullar, Indian Journal of Science and Technology **9** (39) (2016).
DOI: https://doi.org/10.17485/ijst/2016/v9i39/101403

[20] L. Li, Z. Du, X. Sheng, M. Zhao, L. Song, B. Han, X. Li, International Journal of Pressure Vessels and Piping **199**, 104748 (2022).
DOI: https://doi.org/10.1016/j.ijpvp.2022.104748

[21] A. Higelin, S. Le Manchet, G. Passot, et al., Weld World **66**, 1503-1519 (2022).
DOI: https://doi.org/10.1007/s40194-022-01326-0

[22] A. Rokanopoulou, P. Skarvelis, G.D. Papadimitriou, Weld World **63**, 3-10 (2019). DOI: https://doi.org/10.1007/s40194-018-0660-0

[23] G. Sravanthi, S. Ambuj, Iranian Journal of Materials Science and Engineering **1**, 9, (2022).

[24] E. Mortazavi, R.A. Najafabadi, A. Meysami, J. Iron Steel Res. Int. **24**, 1248-1253 (2017).
DOI: https://doi.org/10.1016/S1006-706X(18)30024-4

[25] A.K. Maurya, C. Pandey, R. Chhibber, International Journal of Pressure Vessels and Piping **192**, 104439 (2021).
DOI: https://doi.org/10.1016/j.ijpvp.2021.104439

[26] H. Tan, Z. Wang, Y. Jiang, Y. Yang, B. Deng, H. Song, J. Li, Corrosion Science **55**, 368-377 (2012).
DOI: https://doi.org/10.1016/j.corsci.2011.10.039

[27] E.M. Westin, C.-O.A. Olsson, S. Hertzman, Corrosion Science **50**, 2620-2634 (2008).
DOI: https://doi.org/10.1016/j.corsci.2008.06.024

[28] S.M. Alvarez, A. Bautista, F. Velasco, Corrosion Science **53**, 1748-1755 (2011).
DOI: https://doi.org/10.1016/j.corsci.2011.01.050

[29] J. Nowacki, A. Łukojć, Journal of Materials Processing Technology **164-165**, 1074-1081 (2005).
DOI: https://doi.org/10.1016/j.matchar.2006.02.007

[30] K.W. Chan, S.C. Tjong, Materials **7** (7), 5268-5304 (2014).
DOI: https://doi.org/10.3390/ma7075268

[31] Y. Jiang, H. Tan, Z. Wang, J. Hong, L. Jiang, J. Li, Corrosion Science **70**, 252-259 (2013).
DOI: https://doi.org/10.1016/j.corsci.2013.01.037

[32] N. Ouali, K. Khenfer, B. Belkessa, J. Fajoui, B. Cheniti, B. Idir, S. Branchu, Journal of Materials Engineering and Performance **28**, 4252-4264 (2019).
DOI: https://doi.org/10.1007/s11665-019-04194-w

[33] Y. Hu, Y. Shi, K. Wang, J. Huang, Materials **16** (6), 2289 (2023).
DOI: https://doi.org/10.3390/ma16062289

[34] L. Karlsson, Weld. World **56**, 1-17 (2012).
DOI: https://doi.org/10.1007/BF03321351

[35] J. Verma, R.V. Taiwade, R.K. Khatirkar, S.G. Sapate, A.D. Gaikwad, Trans. Indian Inst. Metals **70**, 225-237 (2017).
DOI: https://doi.org/10.1007/s12666-016-0878-8

[36] R. Mohammed, G.M. Reddy, K.S. Rao, Def. Technol **11**, 237-243 (2015). DOI: https://doi.org/10.1016/j.dt.2015.04.002

[37] P. Prabhu, G. Rajnish, Material Science **29**, 1-9 (2015).
DOI: https://doi.org/10.1051/mfreview/2015032

[38] P. Sathiya. Aravindan, R. Soundararajan, A. Noorul Haq, J. Mater. Sci. **44**, 114-121 (2009).
DOI: https://doi.org/10.1007/s10853-008-3098-8

[39] A.J. Ramirez, J.C. Lippold, S.D. Brandi, Metallurgical and Materials Transactions A **34**, 1575 (2003).
DOI: https://doi.org/10.1007/s11661-003-0304-9

[40] E. Mortazavi, R.A. Najafabadi, A. Meysami. Journal of Iron and Steel Research International **24**, 1248-1253 (2017).
DOI: https://doi.org/10.1016/S1006-706X(18)30024-4

[41] G. Aman, A.K. Baskaran, S. Bhushan, K.K. Rajesh, The Indian Institute of Metals, (2018).
DOI: https://doi.org/10.1007/s12666-018-1294-z